Valley-Polarized Quantum Anomalous Hall Effect in Silicene

Hui Pan,[1] Zhenshan Li,[1] Cheng-Cheng Liu,[2] Guobao Zhu,[3] Zhenhua Qiao,[4,5,6,*] and Yugui Yao[2,†]
[1]Department of Physics, Beihang University, Beijing 100191, China
[2]School of Physics, Beijing Institute of Technology, Beijing 100081, China
[3]Department of Physics, Heze University, Heze, Shandong 274015, China
[4]Department of Physics, University of Science and Technology of China, Hefei, Anhui 230026, China
[5]ICQD, Hefei National Laboratory for Physical Sciences at Microscale, University of Science and Technology of China, Hefei, Anhui 230026, China
[6]Department of Physics, The University of Texas at Austin, Austin, Texas 78712, USA
(Received 22 April 2013; published 12 March 2014)

We find theoretically a new quantum state of matter—the valley-polarized quantum anomalous Hall state in silicene. In the presence of Rashba spin-orbit coupling and an exchange field, silicene hosts a quantum anomalous Hall state with Chern number $\mathcal{C} = 2$. We show that through tuning the Rashba spin-orbit coupling, a topological phase transition results in a valley-polarized quantum anomalous Hall state, i.e., a quantum state that exhibits the electronic properties of both the quantum valley Hall state (valley Chern number $\mathcal{C}_v = 3$) and quantum anomalous Hall state with $\mathcal{C} = -1$. This finding provides a platform for designing dissipationless valleytronics in a more robust manner.

DOI: 10.1103/PhysRevLett.112.106802 PACS numbers: 73.43.-f, 71.70.Ej, 73.22.-f, 85.75.-d

Silicene, the counterpart of graphene [1] for silicon, has a honeycomb geometry and low-buckled structure. Due to its novel electronic properties, such as a special Dirac-cone structure in the low-energy spectrum, silicene has attracted much attention both theoretically and experimentally [2–9]. Distinct from graphene, silicene possesses a stronger intrinsic spin-orbit coupling (SOC) and a considerable bulk band gap can open at the Dirac points. Therefore, silicene becomes a good candidate to realize the quantum spin Hall state [3,4], a quantized response of a transverse spin current to an electric field [10–13]. On the other hand, a tunable extrinsic Rashba SOC from the mirror symmetry breaking about the silicene plane destroys this effect [10,11]. Interestingly, we theoretically show below that this helps establish another striking topological effect—the quantum anomalous Hall effect (QAHE) [14–20]. Unlike the quantum Hall effects from Landau-level quantization, the QAHE originates from the joint effects of SOC and local magnetization. Although the QAHE has been proposed for over 20 years, there was only evidence of its realization in a magnetic topological insulator until recently [20].

Similar to real spin, valleys K and K' in honeycomb structures provide another tunable binary degree of freedom to design valleytronics. By breaking the inversion symmetry, e.g., by the introduction of staggered AB sublattice potentials, a bulk band gap opens to host a quantum valley Hall effect (QVHE) [21–26] characterized by a valley Chern number $\mathcal{C}_v = \mathcal{C}_K - \mathcal{C}_{K'}$. Besides extrinsic Rashba SOC, intrinsic Rashba SOC also exists in silicene due to its low-buckled structure. Considering that intrinsic and extrinsic Rashba SOCs in silicene give different responses at valleys K and K', it is natural to expect that a new topological phase may arise due to the coexistence of intrinsic and extrinsic Rashba SOCs in silicene. Below, we show that the QVHE can also be produced from the interplay between intrinsic and extrinsic Rashba SOCs in silicene without introducing staggered AB sublattice potentials, and the striking properties of both the QAHE and the QVHE can coexist in our new discovered topological phase.

In this Letter, we report the theoretical finding of a valley-polarized quantum anomalous Hall (QAH) phase in silicene. When the time-reversal symmetry is broken from the exchange field, the competition between intrinsic and extrinsic Rashba SOCs results in a new topological phase; i.e., a bulk band gap closing and reopening occurs with the increase of extrinsic Rashba SOC. Through analyzing the resulting Berry curvatures of the occupied valence bands, we show that the nonzero Chern number directly indicates a QAH phase. Surprisingly, we further find that valleys K and K' contribute to different Chern numbers, i.e., $\mathcal{C}_K = 1$ but $\mathcal{C}_{K'} = -2$. This imbalance signals a quantum va]lley Hall phase with valley Chern number $\mathcal{C}_v = 3$. Our finding not only provides a platform to design low-power electronics but also advances the application of silicene-based valleytronics.

In the tight-binding approximation, the Hamiltonian for silicene in the presence of SOCs and an exchange field can be written as [3,4]

$$\begin{aligned} H = & -t\sum_{\langle ij\rangle\alpha} c_{i\alpha}^{\dagger} c_{j\alpha} + it_0 \sum_{\langle\langle ij\rangle\rangle\alpha\beta} \nu_{ij} c_{i\alpha}^{\dagger} \sigma_{\alpha\beta}^{z} c_{j\beta} \\ & - it_{SO} \sum_{\langle\langle ij\rangle\rangle\alpha\beta} \mu_{ij} c_{i\alpha}^{\dagger} (\boldsymbol{\sigma} \times \hat{\boldsymbol{d}}_{ij})_{\alpha\beta}^{z} c_{j\beta} \\ & + it_R \sum_{\langle ij\rangle\alpha\beta} c_{i\alpha}^{\dagger} (\boldsymbol{\sigma} \times \hat{\boldsymbol{d}}_{ij})_{\alpha\beta}^{z} c_{j\beta} + M \sum_{i\alpha\beta} c_{i\alpha}^{\dagger} \sigma_{\alpha\beta}^{z} c_{i\beta}, \end{aligned} \quad (1)$$

where $c^{\dagger}_{i\alpha}(c_{i\alpha})$ is a creation (annihilation) operator for an electron with spin α on site i. The first term represents the nearest neighbor hopping term with hopping energy t. The second term is the effective SOC involving the next-nearest neighbor hopping with amplitude t_0. $\nu_{ij} = \boldsymbol{d}_j \times \boldsymbol{d}_i/|\boldsymbol{d}_j \times \boldsymbol{d}_i|$, where $\boldsymbol{d}_i$ and $\boldsymbol{d}_j$ are two nearest neighbor bonds connecting the next-nearest neighbor sites. The summation over $\langle\cdots\rangle$ ($\langle\langle\cdots\rangle\rangle$) runs over all the nearest (next-nearest) neighbor sites. The third and fourth terms are respectively the intrinsic and extrinsic Rahsba SOC with t_{SO} and t_R the corresponding strengths. $\hat{\boldsymbol{d}}_{ij} = \boldsymbol{d}_{ij}/|\boldsymbol{d}_{ij}|$, where $\boldsymbol{d}_{ij}$ represents a vector from site j to i, and $\mu_{ij} = \pm 1$ for an A or B site. The last term is an exchange field M, which arises from the interaction with a magnetic substrate.

By transforming the real-space Hamiltonian in Eq. (1) into a 4×4 matrix $H(\boldsymbol{k})$ for each crystal momentum $\boldsymbol{k}$ on the basis of $\{\psi_{A\uparrow}, \psi_{A\downarrow}, \psi_{B\uparrow}, \psi_{B\downarrow}\}$, the band structure of bulk silicene can be numerically obtained by diagonalizing $H(\boldsymbol{k})$. Figures 1(a)–1(f) plot the evolution of the bulk band structure along with the increase of extrinsic Rashba SOC t_R. Thanks to the absence of intervalley scattering, valleys K and K' remain good quantum numbers and distinguishable. In the absence of extrinsic Rashba SOC $t_R/t = 0$, one can see that bulk band gaps open at valleys K and K'. When the Fermi level lies inside the bulk energy gap, it is known that this insulating state is a QAH insulator, which is characterized by a nonzero Chern number $\mathcal{C}$ [27–29] calculated from

$$\mathcal{C} = \frac{1}{2\pi}\sum_n \int_{BZ} d^2\mathbf{k}\Omega_n, \tag{2}$$

where Ω_n is the momentum-space Berry curvature for the nth band [27,30,31]

$$\Omega_n(\mathbf{k}) = -\sum_{n' \neq n} \frac{2\mathrm{Im}\langle\psi_{nk}|v_x|\psi_{n'k}\rangle\langle\psi_{n'k}|v_y|\psi_{nk}\rangle}{(\varepsilon_{n'} - \varepsilon_n)^2}. \tag{3}$$

The summation is over all occupied valence bands in the first Brilloin zone below the bulk energy gap, and $v_{x(y)}$ is the velocity operator along the $x(y)$ direction. The absolute value of $\mathcal{C}$ corresponds to the number of gapless chiral edge states along any edge of the two-dimensional system. When $t_R/t = 0$, the Chern number obtained from the tight-binding Hamiltonian is $\mathcal{C} = 2$. Furthermore, by evaluating the Berry curvature and then integrating over the neighborhood of the K or K' point, we can obtain the Chern number of each valley based on the continuum model Hamiltonian. The Chern number contribution of each valley is found to be $\mathcal{C}_K = \mathcal{C}_{K'} = 1$. In this case, the corresponding valley Chern number $\mathcal{C}_v = \mathcal{C}_K - \mathcal{C}_{K'}$ is vanishing. As plotted in Figs. 1(b)–1(f), when the extrinsic Rashba SOC gradually increases from $t_R/t = 0.01$ to $t_R/t = 0.09$, we find that the bulk band gap at valley K always increases. To our surprise, the corresponding bulk band gap at valley K' closes and reopens twice, signaling two possible topological phase transitions.

Let us now explore the topological properties of the resulting two phases based on the Chern number calculation described in Eq. (2). In the first phase after the gap reopening shown in Fig. 1(d), the Chern number is obtained to be $\mathcal{C} = -1$. Since the bulk gap near valley K does not close, the resulting Chern number remains unchanged as $\mathcal{C}_K = 1$. However, the corresponding contribution from valley K' becomes $\mathcal{C}_{K'} = -2$. Naturally, this imbalance of the Chern number contributions from valleys K and K' gives rise to a nonzero valley Chern number $\mathcal{C}_v = 3$. This means that the new topological insulating effect is both a

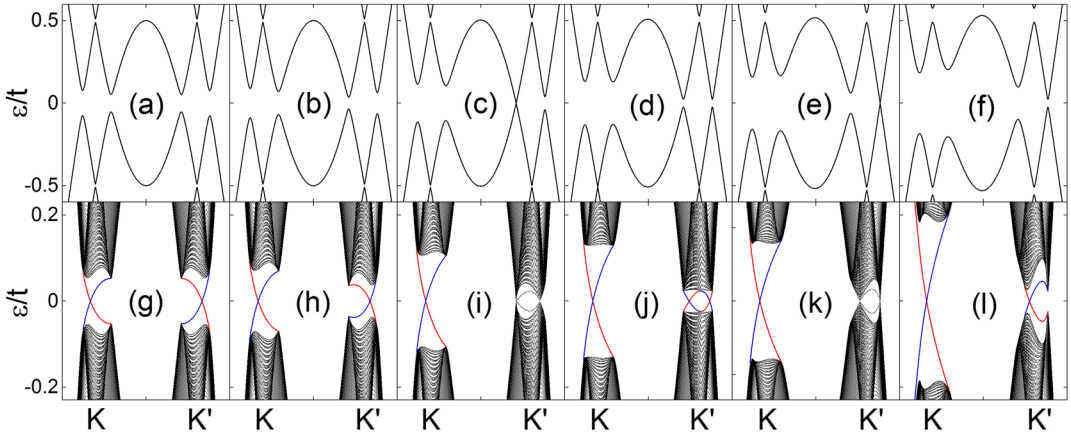

FIG. 1 (color online). Evolution of band structures of the bulk [(a)–(f)] and zigzag-terminated [(g)–(l)] silicene as a function of extrinsic Rashba SOC t_R at fixed intrinsic Rashba SOC t_{SO} and exchange field M. (a) $t_R = 0$. Bulk energy gaps open around the K and K' Dirac points. The size of the bulk gap near valley K is exactly the same as that near valley K'. (b)–(f) $t_R/t = 0.01, 0.031, 0.045, 0.067, 0.09$, respectively. Along with the increasing of t_R, the bulk gap around valley K gradually increases, while the bulk gap near valley K' closes twice [see panels (c) and (e)] and reopens twice [see panels (d) and (f)]. (g)–(l) The valley-associated gapless edge modes at valley K is unchanged, but those for valley K' change; i.e., there are two or one pair of edge modes after the bulk gap reopens. Colors are used to label the edge modes localized at opposite boundaries. Other parameters are set to be $t_0/t = 0.002$, $t_{SO}/t = 0.08$, and $M/t = 0.5$.

QAHE and a QVHE. In the presence of short-range disorders, intervalley scattering is inevitable, e.g., at the upper boundary, edge mode A can be easily scattered back into mode D (or F), and at the bottom boundary edge mode B can be scattered back into mode C (or E) [see Fig. 2(d)]. Therefore, only one pair of edge modes F (or D) and E (or C) can survive due to the protection from spatial separation. In this case, the Chern numbers at valley K and valley K' are respectively $\mathcal{C}_K = 0$ and $\mathcal{C}_{K'} = -1$. The total Chern number is still $\mathcal{C} = -1$ while the valley Chern number becomes $\mathcal{C}_v = 1$. To sum up, under any kind of disorder, our proposed state is a QAH state exhibiting a net valley-polarized current. For simplicity, hereinafter we name it a valley-polarized QAH state. To our knowledge, this is the first time such a phase is reported. To further explore this new phase, in Fig. 2(a) we show the contour of its Berry curvature distribution in the (k_x, k_y) plane. Figure 2(b) plots the Berry curvature as a function of k_x at fixed $k_y = 2\pi/\sqrt{3}$. One can find that the Berry curvatures are mainly localized around the valley points, and obviously the Berry curvature density near valley K is different from that near valley K'. This is a direct consequence of the inequality of the Chern number carried by valley K and K'. In another new phase after the second topological phase transition for even larger t_R [see Fig. 1(f)], the Chern number becomes $\mathcal{C} = 2$ again, where $\mathcal{C}_K = \mathcal{C}_{K'} = 1$ and the corresponding $\mathcal{C}_v = 0$, indicating that this phase is the conventional QAH state. In this way, we have realized a Chern-number-tunable QAHE by controlling the extrinsic Rashba SOC strength.

In addition to the Chern number, the gapless edge mode inside the bulk energy gap provides a more intuitional picture to characterize the QAHE. Figures 1(g)–1(l) plot the one-dimensional band structure of a zigzag-terminated silicene ribbon. One can observe that at valley K there is always one pair of edge modes for any extrinsic Rashba SOC strength, while at valley K' the corresponding edge modes vary along with the topological phase transitions, i.e., after the first and second topological phase transitions there are respectively two and one pair of edge modes. To better reflect the special properties of the valley-polarized QAH phase, in Fig. 2(c) we provide the magnified band structure of Fig. 1(j) to analyze the edge modes labeled A-F. It can be seen that the pair of edge bands labeled A and B connect the conduction band with the valance band at valley K, whereas the other two pairs of edge bands labeled C, D, E, and F connect the conduction band with the valence band at valley K'. Through studying the wave function distribution of the gapless edge states inside the bulk band gap shown in Fig. 2(c) and from the energy dispersion, we find that the edge modes of the valley-polarized QAHE have the form plotted in Fig. 2(d): (1) there are three edge states localized at each boundary, (2) for the upper (lower) boundary, two edge states encoded with valley K' propagate from right (left) to left (right) while one encoded with valley K counterpropagates from left (right) to right (left), and (3) a valley-polarized edge current is produced.

Below, we present a simple theory to reveal the physics behind the formation of this valley-polarized QAHE through strictly solving the low-energy continuum model Hamiltonian. By expanding the tight-binding Hamiltonian shown in Eq. (1) in the vicinity of valleys K and K', a four band low-energy Hamiltonian can be written as

$$H = v(\eta\sigma_x k_x + \sigma_y k_y)\mathbf{1}_s + \eta\lambda_0\sigma_z s_z + \lambda_{SO}\sigma_z(k_y s_x - k_x s_y) + \lambda_R(\eta\sigma_x s_y - \sigma_y s_x) + M\mathbf{1}_\sigma s_z, \quad (4)$$

where $\eta = \pm 1$ label valley degrees of freedom. $\boldsymbol{\sigma}$ and $\mathbf{s}$ are Pauli matrices representing, respectively, the AB-sublattice and spin degrees of freedom. The Fermi velocity, effective SOC, and intrinsic and extrinsic Rashba SOC are given by $v = \sqrt{3}t/2$, $\lambda_0 = 3\sqrt{3}t_0$, $\lambda_{SO} = 3t_{SO}/2$, and $\lambda_R = 3t_R/2$, respectively. Through diagonalizing Eq. (4), the energy spectrum can be expressed as [32]

$$\varepsilon^2_{1,2,3,4} = M^2 + k^2v^2 + 2\lambda_R^2 + k^2\lambda_{SO}^2 \pm 2\sqrt{\lambda_R^4 + k^2(M^2v^2 - 2\eta M v\lambda_R\lambda_{SO} + \lambda_R^2(v^2 + \lambda_{SO}^2))}, \quad (5)$$

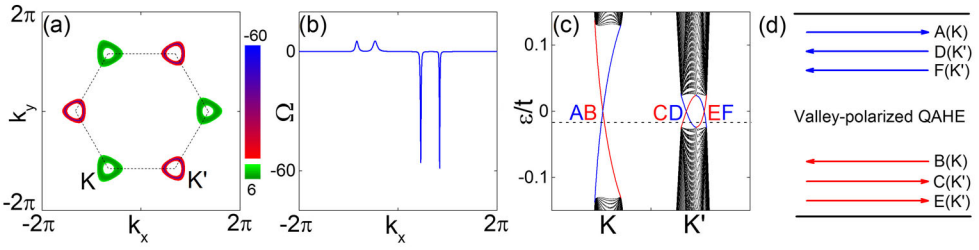

FIG. 2 (color online). (a) Contour of Berry curvature distribution in (k_x, k_y) plane for the valley-polarized QAHE. (b) Berry curvature distribution as a function of k_x at fixed $k_y = 2\pi/\sqrt{3}$. (c) The band structure of zigzag-terminated silicene exhibiting the valley-polarized QAHE [same as that in Fig. 1(j)], where colors are used to label the edge modes localized at opposite boundaries. (d) Valley-associated edge modes for the valley-polarized QAHE.

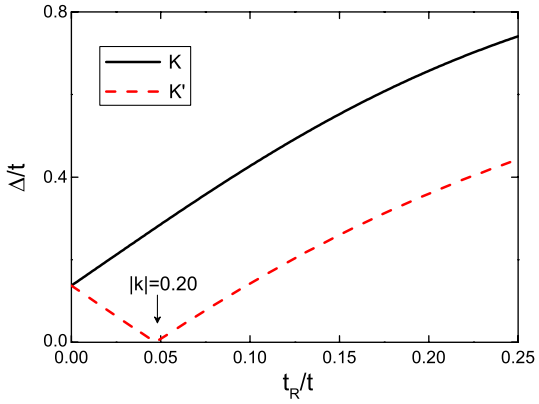

FIG. 3 (color online). Bulk band gap Δ around valleys K and K' as a function of extrinsic Rashba SOC t_R based on Eq. (5). Solid and dashed lines correspond, respectively, to valleys K and K'. Other parameters are the same as those in Fig. 1.

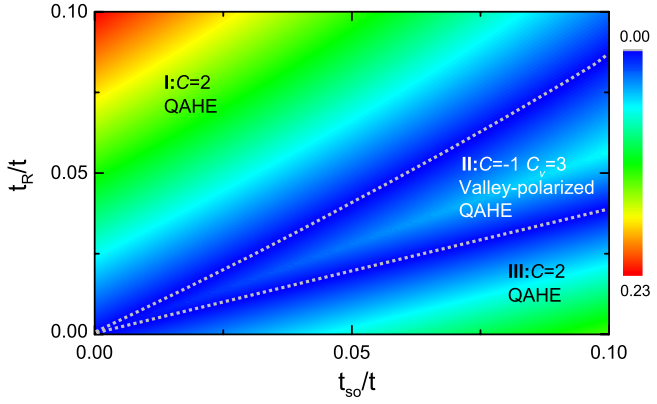

FIG. 4 (color online). Phase diagram in the (t_{SO}, t_R) plane. The dotted lines separate three topological phases for the single layer silicene, and colors are used to indicate the size of the bulk band gap. In phase I and phase III, the Chern numbers are identical $\mathcal{C} = 2$. While in phase II, the Chern number and valley Chern number are $\mathcal{C} = -1$ and $\mathcal{C}_v = 3$, respectively. Other parameters are the same as those in Fig. 1.

where $\varepsilon_1 = -\varepsilon_4$ $(\varepsilon_2 = -\varepsilon_3)$ correspond to high (low) energies. When the extrinsic Rashba term is turned off, i.e., $\lambda_R = 0$, the four eigenenergies become valley independent. Therefore, the contribution from each valley is identical, giving rise to a nonpolarized QAHE. After turning on the extrinsic Rashba term, we find that for valley K $(\eta = +1)$, $\varepsilon_2 = -\varepsilon_3 < 0$ is valid for any λ_R, signaling no band gap inversion, while for valley K' $(\eta = -1)$, $\varepsilon_2 = \varepsilon_3 = 0$ can be satisfied for a certain extrinsic Rashba SOC strength. At $k = 0$, the four eigenenergies are separated. Therefore, the gap closing occurs at a finite momentum k. To verify our analysis, in Fig. 3 we plot the band gap evolution as a function of extrinsic Rashba SOC t_R for both valleys K and K'. One can observe that the band gap for valley K always opens, indicating that the phase is not changed. But for valley K', the band gap closes and reopens at a critical t_R, indicating that a topological phase transition occurs near valley K' at $|k| = 0.20$ [33]. The topologically different responses of valleys K and K' arise from the interplay between the intrinsic and extrinsic Rashba SOCs. As shown in the third term of Eq. (4), the momentum-related intrinsic Rashba SOC couples with the pseudospin degree of freedom of the AB sublattice, which produces a varying staggered potential in the momentum space, and usually the AB staggered sublattice potential can induce a QVHE [21,22]. The fourth term in Eq. (4) is the valley-dependent extrinsic Rashba SOC, which can lead to the conventional QAHE in the presence of an exchange field [17]. Therefore, the competition between the extrinsic and intrinsic Rashba SOCs results in the coexistence of the QAHE and the QVHE, giving rise to the newly proposed valley-polarized QAHE.

Finally, we provide a phase diagram in the (t_{SO}, t_R) plane. Figure 4 clearly shows that there are three topological phases separated by two dotted lines representing the topological phase boundaries. Here, we use colors to signify the size of the corresponding bulk band gap. From the Chern number calculation, we show that the Chern number in phase I is identical to that in phase III, i.e., $\mathcal{C} = 2$. However, in phase II the Chern number is $\mathcal{C} = -1$ and the valley Chern number is $\mathcal{C}_v = 3$, which is exactly the newly found valley-polarized QAHE.

In summary, through tuning the Rashba spin-orbit coupling in silicene, we numerically find a new topological phase—the valley-polarized quantum anomalous Hall state. Different from the conventional quantum anomalous Hall state, the new topological phase has not only a quantized Chern number $\mathcal{C} = -1$, but also a nonzero valley Chern number $\mathcal{C}_v = 3$. Therefore, it possesses the properties of both the quantum anomalous Hall effect and the quantum valley Hall effect, and can be considered as a good candidate for designing dissipationless valleytronics. The Rashba spin-orbit coupling can serve as a topological switch to drive silicene from a conventional quantum anomalous Hall phase to a valley-polarized quantum anomalous Hall phase, which can be realized by controlling the adatom coverage in silicene.

This work was financially supported by the MOST Project of China (Grants No. 2014CB920903 and No. 2011CBA00100), the NSFC (Grants No. 11174022, No. 11174337, and No. 11225418), and the NCET program of MOE (Grant No. NCET-11-0774). Z. Q. was financially supported by USTC Startup, Bairen Program of CAS, and NNSFC (Grant No. 91021019).

*qiao@ustc.edu.cn
†ygyao@bit.edu.cn

[1] K. S. Novoselov *et al.*, Science **306**, 666 (2004).

[2] B. Lalmi, H. Oughaddou, H. Enriquez, A. Kara, S. Vizzini, B. Ealet, and B. Aufray, Appl. Phys. Lett. **97**, 223109 (2010).
[3] C.-C. Liu, W. Feng, and Y. Yao, Phys. Rev. Lett. **107**, 076802 (2011).
[4] C. C. Liu, H. Jiang, and Y. G. Yao, Phys. Rev. B **84**, 195430 (2011).
[5] P. Vogt, P. De Padova, C. Quaresima, J. Avila, E. Frantzeskakis, M. C. Asensio, A. Resta, B. Ealet, and G. Le Lay, Phys. Rev. Lett. **108**, 155501 (2012).
[6] A. Fleurence, R. Friedlein, T. Ozaki, H. Kawai, Y. Wang, and Y. Yamada-Takamura, Phys. Rev. Lett. **108**, 245501 (2012).
[7] M. Ezawa, Phys. Rev. Lett. **109**, 055502 (2012).
[8] L. Chen, C. C. Liu, B. Feng, X. He, P. Cheng, Z. Ding, S. Meng, Y. G. Yao, and K. Wu, Phys. Rev. Lett. **109**, 056804 (2012).
[9] W. F. Tsai, C. Y. Huang, T. R. Chang, H. Lin, H. T. Jeng, and A. Bansil, Nat. Commun. **4**, 1500 (2013).
[10] C. L. Kane, and E. J. Mele, Phys. Rev. Lett. **95**, 146802 (2005).
[11] C. L. Kane, and E. J. Mele, Phys. Rev. Lett. **95**, 226801 (2005).
[12] M. Z. Hasan, and C. L. Kane, Rev. Mod. Phys. **82**, 3045 (2010).
[13] X.-L. Qi and S.-C. Zhang, Rev. Mod. Phys. **83**, 1057 (2011).
[14] M. Onoda and N. Nagaosa, Phys. Rev. Lett. **90**, 206601 (2003).
[15] N. Nagaosa, J. Sinova, S. Onoda, A. H. MacDonald, and N. P. Ong, Rev. Mod. Phys. **82**, 1539 (2010).
[16] R. Yu, W. Zhang, H.-J. Zhang, S.-C. Zhang, X. Dai, and Z. Fang, Science **329**, 61 (2010).
[17] Z. H. Qiao, S. A. Yang, W. X. Feng, W.-K. Tse, J. Ding, Y. G. Yao, J. Wang, and Q. Niu, Phys. Rev. B **82**, 161414(R) (2010).
[18] W.-K. Tse, Z. H. Qiao, Y. G. Yao, A. H. MacDonald, and Q. Niu, Phys. Rev. B **83**, 155447 (2011).
[19] J. Ding, Z. H. Qiao, W. X. Feng, Y. G. Yao, and Q. Niu, Phys. Rev. B **84**, 195444 (2011).
[20] C. Z. Chang *et al.*, Science **340**, 167 (2013).
[21] D. Xiao, W. Yao, and Q. Niu, Phys. Rev. Lett. **99**, 236809 (2007).
[22] W. Yao, D. Xiao, and Q. Niu, Phys. Rev. B **77**, 235406 (2008).
[23] I. Martin, Ya. M. Blanter, and A. F. Morpurgo, Phys. Rev. Lett. **100**, 036804 (2008).
[24] W. Yao, S. A. Yang, and Q. Niu, Phys. Rev. Lett. **102**, 096801 (2009).
[25] Z. H. Qiao, W.-K. Tse, H. Jiang, Y. G. Yao, and Q. Niu, Phys. Rev. Lett. **107**, 256801 (2011); Z. H. Qiao, J. Jung, Q. Niu, and A. H. MacDonald, Nano Lett. **11**, 3453 (2011); J. Jung, Z. H. Qiao, Q. Niu, and A. H. MacDonald, *ibid.*. **12**, 2936 (2012).
[26] H. Z. Lu, W. Yao, D. Xiao, and S. Q. Shen, Phys. Rev. Lett. **110**, 016806 (2013).
[27] D. J. Thouless, M. Kohmoto, M. P. Nightingale, and M. den Nijs, Phys. Rev. Lett. **49**, 405 (1982).
[28] M. Kohmoto, Ann. Phys. (N.Y.) **160**, 343 (1985).
[29] D. Xiao, M. C. Chang, and Q. Niu, Rev. Mod. Phys. **82**, 1959 (2010).
[30] M. C. Chang, and Q. Niu, Phys. Rev. B **53**, 7010 (1996).
[31] Y. G. Yao, L. Kleinman, A. H. MacDonald, J. Sinova, T. Jungwirth, D. S. Wang, E. G. Wang, and Q. Niu, Phys. Rev. Lett. **92**, 037204 (2004).
[32] The effective SOCλ_0 is negligible, because it is very small compared with other parameters.
[33] It is noteworthy that there is only one topological phase transition in Fig. 3. The reason is that the second phase transition cannot be captured by the low-energy picture.